J. Synchrotron Rad. (1998). **5**, 797–800

Multi-segmented piezoelectric mirrors as active/adaptive optics components

Riccardo Signorato,* Olivier Hignette and José Goulon

ESRF, BP 220, 38043 Grenoble CEDEX, France.
E-mail: signorato@esrf.fr

(*Received 5 August 1997; accepted 28 October 1997*)

The angular acceptance of piezoelectric (Pzt) bimorph mirrors is limited by the maximum length of commercially available Pzt ceramic plates. To overcome this limit and manufacture longer devices, several ($2n$ + 1) 150 mm-long bimorph Pzt stacks were assembled side-to-side. Two prototype mirrors, 450 (n = 1) and 750 (n = 2) mm long, were designed, assembled, polished and optically characterized. They are fully UHV compatible and are now installed in the monochromatic section of the ESRF beamlines ID26 and ID32. Both mirrors cover the full range of required bending radii (1 km concave–3.5 km convex). Junctions between segments do not spoil the optical surface quality. The surface slope error r.m.s. can be kept well below 1 arcsec over the full bending range. Adaptive compensation for low-frequency figure errors was shown to be easy and reliable. After compensation, residual shape errors are of the order of 40 nm r.m.s. over 700 mm.

Keywords: multi-segmented piezoelectric mirrors; active/adaptive optics.

1. Introduction

There is a clear interest within the synchrotron radiation community in dynamically bendable mirrors. The adjustability of the focusing process adds flexibility to the beamline optics, allowing changes in the grazing-incidence angle or in the mirror-to-sample distance. Several systems are routinely exploited to deform an optical element (mirrors/multilayers/crystals) by applying mechanical bending momenta. At the ESRF an alternative approach based on piezoelectric bimorph mirrors (PBMs) (Susini *et al.*, 1995, 1996) has been proposed. PBMs combine simplicity, ease of use and versatility together with an attractive overall price. A customized design for PBMs (L = 150–200 mm, W = 40–45 mm, T = 15–18 mm) was optimized and a series of ten mirrors was manufactured (Susini *et al.*, 1996). This design is inherently limited by the small angular acceptance at grazing incidence due to the restricted length of the mirrors.

Given the non-availability of longer Pzt ceramic plates, we decided to design a new type of multisegmented mirror by assembling side-to-side several 150 mm PBMs between two long fused-silica plates.

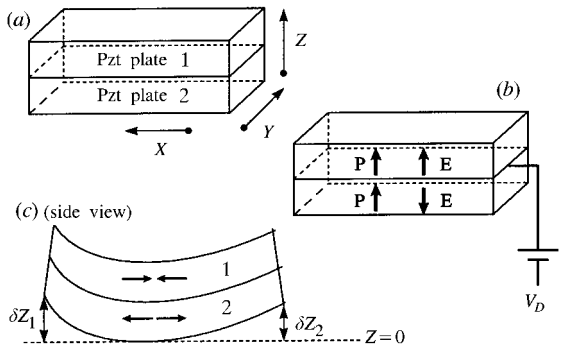

Figure 1
(*a*)–(*c*) Bending principle of PBMs (see text). For clarity the two neutral silicon plates are not represented.

2. Piezoelectric bimorph mirrors: bending principle

A nice feature of PBMs is that the bending mechanism is intrinsic to the mirror itself. PBMs are assembled (Cilas Inc., France) by gluing together two pairs of bilayers (Fig. 1*a*) consisting of an active element, made from zirconate lead titanate Pzt ceramic and a thin neutral silicon plate which is then polished. The two Pzt ceramics in each PBM are polarized normal to their surface and their polarization vectors ($\mathbf{P}_1$ and $\mathbf{P}_2$) are parallel (Fig. 1*b*). A thin (5000 Å) driving gold electrode (El_D) is deposited at the Pzt–Pzt bonding interface. The ground electrode (El_G) is situated at each of the two ceramic/silicon interfaces. When a driving voltage (V_D) is applied at El_D one Pzt shrinks while the other expands. This differential expansion results in a bending of the whole assembly (see Figs. 1*b* and 1*c*). No anticlastic effect is present.

The longitudinal (meridional) and transversal (sagittal) radii of curvature ($R_{m,s}$) are approximately equal and inversely proportional to V_D. As a result of their symmetric construction, PBMs are, in practice, insensitive to temperature drifts.

3. Segmented piezoelectric bimorph mirrors: conceptual design

The basic idea for segmented PBMs is to assemble side-to-side ($2n$ + 1) 150 mm long Pzt–Pzt sandwiches (segments) between two long fused-silica (Herasil) plates which assure mechanical continuity. Two prototypes were manufactured: a three (n = 1) segment (450 mm: M1) device for beamline ID32 (Comin *et al.*, 1997) and a five (n = 2) segment (750 mm: M2) for ID26 (Signorato *et al.*, 1997) (see Fig. 2). Both devices have been characterized optically and are now operational. Each mirror is kept under vacuum (*ca* 4×10^{-9} mbar – with no bakeout).

3.1. *Mechanical design*

In order to minimize the deformations induced by the segmentation, we used rather thick Herasil plates. To avoid mechanical stresses due to differential expansion between Pzt and fused silica, polymerization of the UHV compatible ceramic glue was achieved at low temperature (333 K). Residual stresses due to assembly are eventually relaxed by ageing the system, *i.e.* by cycling the segmented PBM between ±600 V at 50 Hz for more than 250 h.

3.2. *Electrical design*

Each segment has a separated single control electrode that can be independently driven. The ground electrode is continuous over the whole mirror length as shown in Fig. 2(*b*). An insulating gap is left between two consecutive driving electrodes (see Fig. 2*b*), thus allowing voltage differentials of ±500 V.

3.3. *Optical design*

To lower the high voltage values required to cover the full range of bending radii (R), we decided to polish both mirrors to a

concave shape. The nominal static radius (*i.e.* R_0, the radius at $V_D = 0$) was specified by averaging between the longest and the shortest radii dictated by the geometrical setups. This strategy allowed us to minimize hysteresis and distortions due to excessive bending. According to our specifications, both mirrors had to be polished (SESO Inc., France) to a spherical radius kept between 3 and 5 km and the residual slope error ($sl_{\rm err}$) was expected to be lower than 1 arcsec r.m.s.

Three reflective strips, (i) Cr, (ii) bare and (iii) Pt, are available on each mirror to select different energy cutoffs.

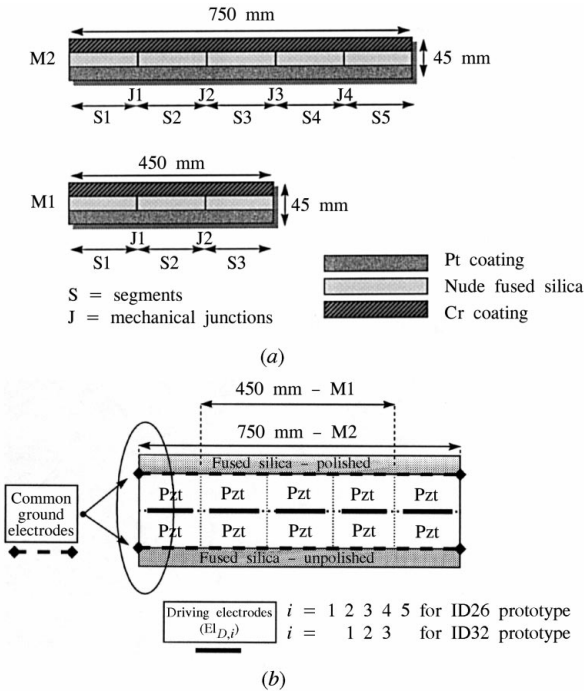

Figure 2
Top (*a*) and side (*b*) view of the two prototype mirrors M1 and M2.

4. Optical metrology

The segmented PBMs can be operated in two different modes: (i) *active* and (ii) *adaptive*. In the active mode all the electrodes are kept at the same potential, thus producing a uniform smooth variation of the bending radius that preserves the initial spherical shape. In the adaptive mode, we are not interested in high-speed wavefront correction (typically, segmented PBMs can be operated at $<10^{-2}$ Hz). We are mainly looking for ultimate precision of the reflecting surface shape (in the few nm r.m.s. range). We then propose the following definition: "A segmented PBM is operated in 'adaptive' mode when its surface is locally modified in order to react to a distortion in the incoming/outcoming wavefront. This distortion can be of static nature (polishing errors, gravity sag) or evolving in time on a sub-Hz scale (thermal bumps due to heat load)."

We have already tested both modes of operation in the ESRF metrology lab. Results are quite encouraging in demonstrating the validity of the segmented PBM concept and the practical feasibility of their adaptive capabilities.

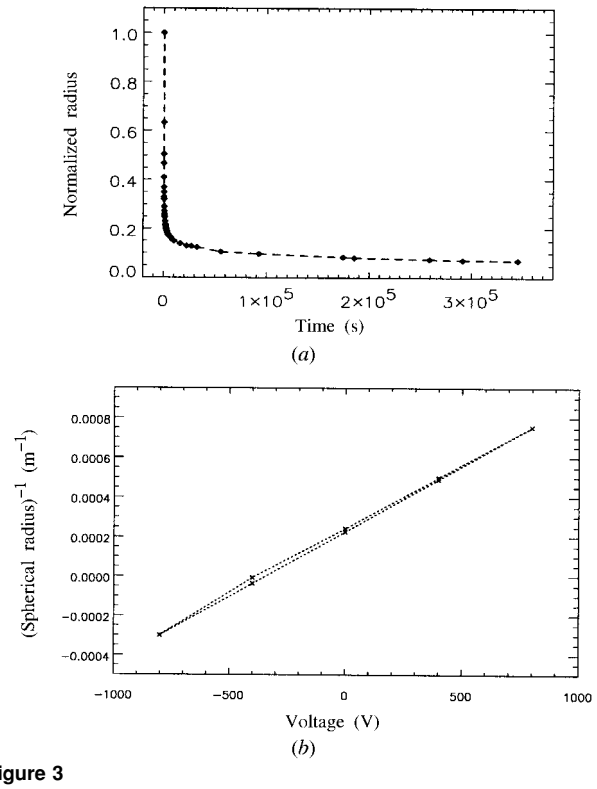

Figure 3
(*a*) Measured creeping on M2. τ is *ca* 150 s. (*b*) Hysteresis effect on the same mirror. Hysteresis is in the 2% range.

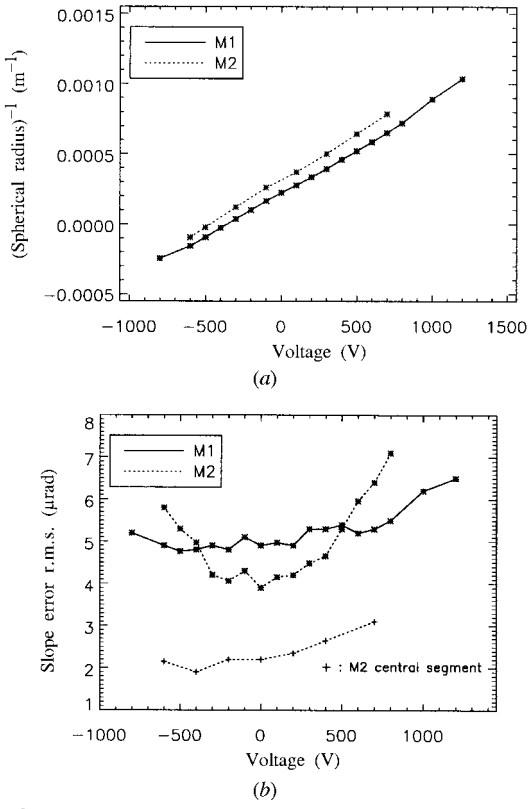

Figure 4
Calibration charts for M1 and M2. Data taken on 445 mm for M1 and 715 mm for M2. (*a*) 1/*R*. (*b*) Slope errors.

4.1. *Creep and hysteresis characterization*

These effects are intrinsic to any Pzt ceramic device and must be carefully characterized if a closed correction loop is not available. To carry out creep measurements a Shack–Hartmann wavefront sensor (SH) (manufactured according to ESRF specifications by Visionix Ltd, Israel) was preferred to the ESRF long trace profiler (LTP) because of its faster acquisition time (SH, 50 ms; LTP, >1 min). Creeping is quite evident (see Fig. 3*a*), but the time constant (τ) is rather short (*ca* 2.5 min). After 10 min (*ca* 4τ) from the HV enabling, the system does not, in practice, evolve any more and shows remarkable long-term stability (without any feedback system!).

Hysteresis was characterized to be in the 2% range (Fig. 3*b*).

4.2. *'Active' metrology*

A calibration curve was determined for each segmented PBM as a function of V_D (Fig. 4*a*). Both segmented PBMs show a linear V_D *versus* $1/R$ calibration chart. On M1 the slope error does not evolve significantly on increasing V_D. The increase measured on M2 for $|V_D| > 500$ V is compensated by the reduction of the beam footprint, as the central part of each segmented PBM always exhibits figure errors in the 1.5–2.0 µrad r.m.s. range. Junction effects are present in all LTP measurements. Nevertheless, they do not evolve with V_D and a profile taken at 0 V (see Fig. 5) fully characterizes them. The maximum amplitude of the bumps at each discontinuity (<0.1 µm peak-to-valley) is one order of magnitude smaller than the polishing errors.

4.3. *'Adaptive' metrology*

A general purpose estimation and control matrix algorithm can be applied to segmented PBMs to optimize their performance from wavefront distortion measurements. We tested this algorithm to compensate locally for static distortions due to polishing: LTP measurements were used to detect deformations from ideally spherical surfaces. We achieved our goal and excellent results were obtained. In order to apply the algorithm one has to define a local *linear* relationship between the five $V_{D,i}$ and a physical quantity that can be measured. A mirror deformation can be characterized by means of its curvature R and related residuals (slope and shape errors – denoted hereafter as $sl/sh_{\rm err}$) obtained by subtracting a linear best fit from the raw slope data (Signorato & Sanchez Del Rio, 1997). To linearize the problem, it was necessary to work on $sl_{\rm err}$ and $sh_{\rm err}$, ignoring R.

Starting from a given reference surface of M2, $sl/sh_{\rm err}$ are sampled by the LTP in m points over a longitudinal trace, producing an error vector $\boldsymbol{\delta}\mathbf{f}_0(x_i)$ ($i = 1 \ldots m$). A unit signal $V1$ is then sent sequentially to each electrode, resulting in the associated error vectors $\boldsymbol{\delta}\mathbf{f}_{1\ldots5}(x_i)$. The five vectors $\boldsymbol{\delta}\mathbf{f}_{1\ldots5}(x_i)$–$\boldsymbol{\delta}\mathbf{f}_0(x_i)$ are used to write the *interaction matrix* of the system: **H** (5 by m elements). By knowing **H**, the solution to the least-squares minimization of a given measured distortion $\boldsymbol{\delta}\mathbf{f}_0(x_i)$ is given by:

$$\begin{pmatrix} V_{D,1} \\ V_{D,2} \\ V_{D,3} \\ V_{D,4} \\ V_{D,5} \end{pmatrix} = (H^T H)^{-1} H^T \delta f_0,$$

where ^{T} is the standard notation for the transposed matrix. A pseudo inverse singular value decomposition (SVD) method is used to avoid singularities of **H**.

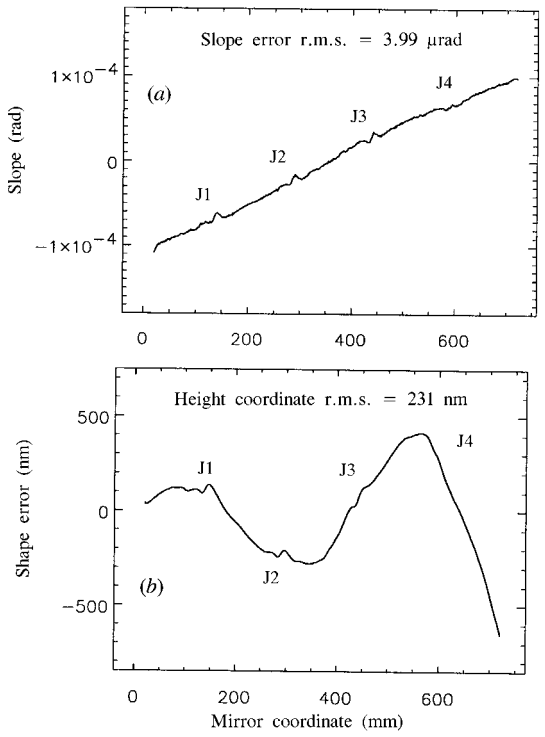

Figure 5
Slope (*a*) and height error (*b*) at 0 V on M2. $R_0 = 3265$ m.

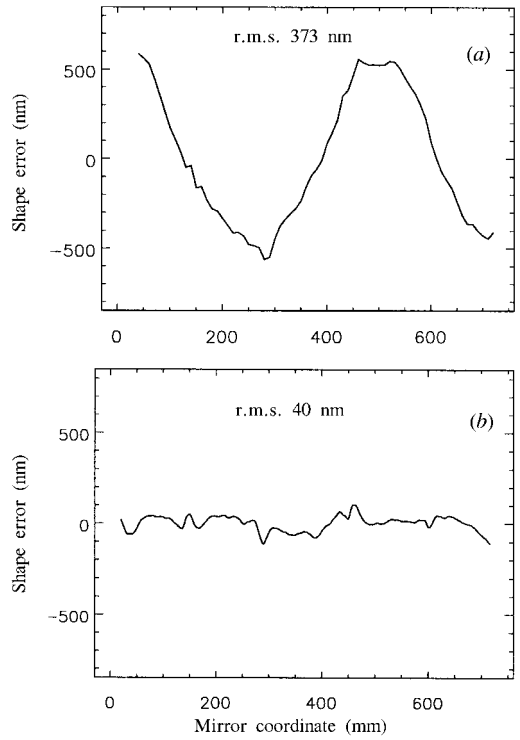

Figure 6
Adaptive correction of low-frequency shape error components due to polishing. (*a*) V_D is set at −450 V on every electrode. (*b*) Effect of the adaptive compensation.

The optimization process can be iterated until the required tolerances are satisfied. We found that generally one or two iterations are enough. To keep R at a fixed value, the sum of the five voltage corrections should be kept constant. Once the corrective differential voltages between the electrodes are set, the focus size will be minimized by applying the same voltage differential on all electrodes, according to the bimorph system calibration curve.

The minimization procedure gave excellent results, illustrated by Fig. 6. A factor of two can be gained on $sl_{\rm err}$ (reduced from 5.81 to 3.12 μrad r.m.s.) and almost one order of magnitude on $sh_{\rm err}$ (reduced from 373 to 40 nm r.m.s.) by selectively attenuating long-period components of the height error.

A method for *in situ* active correction, based on the analysis of the real X-ray wavefront with a scanning slit technique has already been tested on a simpler bendable device (Hignette *et al.*, 1997). The next step, after the commissioning of M1 and M2, will be to couple this procedure with the finer correction capabilities of the segmented PBMs in order to maximize the mirrors *in situ* performance.

RS wishes to thank SESO for financial support during his PhD thesis.

References

Comin, F., Fezzaa, K., Ortega, L., Formoso, V., De Martino, R. & Signorato, R. (1997). *J. Phys. (Paris) IV*, **7**, C2-343–344.

Hignette, O., Freund, A. & Chinchio, E. (1997). *SPIE Proc.* **3152**. In the press.

Signorato, R. & Sanchez Del Rio, M. (1997). *Proc. SPIE*, **3152**. In the press.

Signorato, R., Susini, J., Goulon, J., Gauthier, Ch. & Marion, P. (1997). *J. Phys. (Paris) IV*, **7**, C2-331–332.

Susini, J., Labergerie, D. & Zhang, L. (1995). *Rev. Sci. Instrum.* **66**(2), 2229–2231.

Susini, J., Labergerie, D. & Hignette, O. (1996). *SPIE Proc.* **2856**, 130–144.